Journal of
Synchrotron
Radiation

ISSN 1600-5775

Received 12 January 2014
Accepted 15 April 2014

Tracking extended mucociliary transport activity of individual deposited particles: longitudinal synchrotron X-ray imaging in live mice

Martin Donnelley,[a,b,c]* Kaye S. Morgan,[d] Karen K. W. Siu,[d] Andreas Fouras,[e] Nigel R. Farrow,[a,b,c] Richard P. Carnibella[e] and David W. Parsons[a,b,c]

[a]Respiratory and Sleep Medicine, Women's and Children's Hospital, 72 King William Road, North Adelaide, SA 5006, Australia, [b]Robinson Research Institute, University of Adelaide, SA 5001, Australia, [c]School of Paediatrics and Reproductive Health, University of Adelaide, SA 5001, Australia, [d]School of Physics, Monash University, Clayton, Vic 3800, Australia, and [e]Mechanical and Aerospace Engineering, Monash University, Clayton, Vic 3800, Australia. *E-mail: martin.donnelley@adelaide.edu.au

To assess potential therapies for respiratory diseases in which mucociliary transit (MCT) is impaired, such as cystic fibrosis and primary ciliary dyskinesia, a novel and non-invasive MCT quantification method has been developed in which the transit rate and behaviour of individual micrometre-sized deposited particles are measured in live mice using synchrotron phase-contrast X-ray imaging. Particle clearance by MCT is known to be a two-phase process that occurs over a period of minutes to days. Previous studies have assessed MCT in the fast-clearance phase, ~20 min after marker particle dosing. The aim of this study was to non-invasively image changes in particle presence and MCT during the slow-clearance phase, and simultaneously determine whether repeat synchrotron X-ray imaging of mice was feasible over periods of 3, 9 and 25 h. All mice tolerated the repeat imaging procedure with no adverse effects. Quantitative image analysis revealed that the particle MCT rate and the number of particles present in the airway both decreased with time. This study successfully demonstrated for the first time that longitudinal synchrotron X-ray imaging studies are possible in live small animals, provided appropriate animal handling techniques are used and care is taken to reduce the delivered radiation dose.

Keywords: particles; airway surface; lung; trachea; mucociliary transit; non-invasive; X-ray imaging; phase contrast; mouse; longitudinal; repeat; dose.

1. Introduction and objectives

Mucociliary transport (MCT) is the coordinated beating of cilia, *i.e.* the microscopic hair-like structures that project into the airway surface liquid (ASL) from the surfaces of epithelial cells, that removes deposited pathogens, particulates and mucus from the airways. In cystic fibrosis (CF) airways disease an improperly functioning CF transmembrane conductance regulator (CFTR) ion channel in airway epithelial cells results in ASL dehydration and impaired MCT. Over time this causes retention of pathogens and particulates, increasing mucus obstructions, chronic infection and inflammation, and eventually results in lung failure (Boucher, 2004). In another inherited condition, primary ciliary dyskinesia (PCD), the cilia are immotile or ineffective, resulting in poor MCT, persistent respiratory infections and deteriorating lung function (Chodhari *et al.*, 2004).

A logical method to assess native MCT behaviour, as well as the effectiveness of CF and PCD therapies on that airway surface behaviour, is to directly measure MCT activity by tracking the movement of deposited marker particles. We have developed a novel MCT monitoring method for use *in vivo* in live anaesthetized mice that is based on quantifying the transit rate and behaviour of individual deposited particles using synchrotron phase-contrast X-ray imaging (PCXI) (Donnelley *et al.*, 2009, 2010, 2012). In contrast, conventional *in vivo* MCT measurement methods, such as inhaled radio-tracers, typically measure bulk particle clearance from the airways (Grubb *et al.*, 2004; Donaldson *et al.*, 2007; Livraghi & Randell, 2007; Hua *et al.*, 2010) but are unable to track the motion of *individual* micrometre-sized deposited particles with high spatial or temporal resolution, and therefore cannot assess localized changes in MCT behaviour. The ability to do this should allow identification of early regions of disease, char-

acterization of the heterogeneity underlying bulk MCT and potential assessment of the regionality of drugs designed to alter MCT.

PCXI is ideally suited to non-invasive airway surface imaging in small-animal models. Provided the incident X-ray beam is spatially coherent, increasing the sample-to-detector distance (Snigirev *et al.*, 1995; Cloetens *et al.*, 1996; Wilkins *et al.*, 1996) enhances air-to-tissue interfaces due to the phase changes that are induced by differences in the tissue X-ray refractive indices. Our previous studies have assessed the MCT behaviour of a range of inhaled pollutant particles (Donnelley *et al.*, 2012) as well as the effects of inhaled clinical CF therapeutics on MCT (Donnelley *et al.*, 2014). These studies have also revealed that deposited lead dust, predominantly ranging in size from 5 μm up to 12 μm diameter, with a small number of larger particles present (see Fig. 3 of Donnelley *et al.*, 2010), is a suitable marker for analysing tracheal MCT behaviour *via* PCXI.

In previous experiments we examined the post-deposition behaviour of particles in the ∼20 min after delivery. Although we have visualized and described particle clearance within this short period, the particulates are by no means cleared from the airways. Clearance is known to be a two-phase process, with a fast-clearance phase that removes the bulk of the particles within hours, and a slow-clearance phase that removes additional particles over a period of multiple days (Falk *et al.*, 1999; Hofmann & Asgharian, 2003; Moller *et al.*, 2004). Reductions in radiation dose resulting from recent improvements in detector technology and experimental methodologies now allow the use of repeated-measures study designs to monitor MCT changes in individual animals. Although other researchers seek to perform longitudinal synchrotron X-ray imaging studies (Coan *et al.*, 2010), we are unaware of any reports of repeat-imaging experiments in living animals.

The primary aim of this study was to confirm for the first time the feasibility of performing repeat synchrotron phase-contrast imaging of the same mice over time. The secondary aim was to non-invasively observe and describe the surface activity of live mouse airways at micrometre resolution and to image and quantify changes in individual particle MCT during the slow-clearance phase, for up to 25 h.

2. Methods

The BL20XU undulator beamline at the SPring-8 synchrotron radiation facility in Japan was used for all imaging experiments, under approvals from the Animal Ethics Committees of SPring-8, the Women's and Children's Health Network, and the University of Adelaide.

2.1. Imaging set-up

The imaging set-up was as previously described (Donnelley *et al.*, 2012). Briefly, imaging was performed in the downstream experimental hutch located in the Biomedical Imaging Centre, at a distance of 245 m from the storage ring. Monochromatic 25 keV X-rays and a sample-to-detector distance of ∼1 m were used. Images were captured using a high-resolution X-ray converter (SPring-8 BM3 with a 10 μm-thick scintillator) coupled to a sCMOS detector (pco.edge; PCO Imaging, Michigan, USA) *via* a ×10 microscope objective lens (numerical aperture 0.45). This set-up produced images with an effective isotropic pixel size of 0.56 μm and a field of view of 1.43 mm × 1.2 mm (2560 × 2160 pixels). The incident beam was also limited to this size using slits to reduce the radiation dose to the animals. An ion chamber (S-1329A; Oken, Tokyo, Japan) was placed immediately after the slits to measure the photon flux. Image capture was synchronized with a fast shutter (Uniblitz XRS6 with VMM-T1 timer unit; Vincent Associates, NY, USA) to minimize the dose between exposures. Exposure lengths of 50 ms were used to produce a high signal-to-noise ratio without movement blur.

2.2. Animal preparation

All mice (n = 24 female C57Bl/6, weight ∼18–20 g) were prepared as for previous experiments (Donnelley *et al.*, 2012). Each mouse was anaesthetized with pentobarbital (Somnopentil; Pitman-Moore, Washington Crossing, USA; 100 mg kg^{-1} i.p.) with top-up doses delivered as required to maintain adequate depth of anaesthesia. The fur around the imaging area was removed using surgical clippers (Neuro blade; CareFusion, San Diego, USA) followed by depilatory cream (Nair, Church & Dwight, Australia) to minimize imaging interference. The mice were then intubated using a fibre-optic illuminated guide wire and a 20 Ga i.v. catheter (Insyte; Becton Dickinson, Utah, USA) as an endotracheal (ET) tube. The ET tube was inserted into the trachea such that the tip was approximately half way between the epiglottis and the carina to avoid physically perturbing the more distal imaging region. A small quantity (less than 0.001 g) of lead dust was delivered to the trachea and lungs *via* the ET tube using a Dry Powder Insufflator™ Model DP-4M (Penn-Century; Wyndmoor, PA, USA). Owing to high variability in the particle mass delivered on the first actuation of the air pump, this first output was discarded and the second actuation was used to deliver the sample to the airways (Donnelley *et al.*, 2012). The particle size distribution was as described previously (Donnelley *et al.*, 2012).

Each mouse was then tethered in a custom-designed imaging holder designed to minimize body movements that interfere with high-resolution imaging. The mouse holder was mounted on the hutch sample stage so that the mouse was oriented supine and the X-ray beam passed laterally through the trachea distal to the ET tube tip. The ET tube was attached to a flexiVent small-animal ventilator (SCIREQ; Montreal, Canada), and ventilation was set at 120 breaths min^{-1}, a tidal volume of 15 ml kg^{-1} and ∼3 cm H_2O of PEEP. The flexiVent provided a trigger within each end-expiratory pause. Body temperature was maintained using an infrared heat lamp and monitored *via* a rectal probe. The imaging region was located using as few exposures as possible to minimize the radiation dose delivered.

Mice were randomly assigned to one of three groups; 3 h imaging, 9 h imaging or 25 h imaging (n = 8 per group). These times were chosen to represent a short, moderate and day-long period, and were designed to fit the entire experiment within two days of allocated synchrotron beam time. All groups were imaged after particle delivery (0 h) to determine the baseline particle distribution and MCT behaviour. At baseline, one image was captured every ten breaths (5.5 s) for 1 min and after a 4 min delay this imaging sequence was repeated, producing a total baseline set of 24 images. Mice were then removed from the hutch, extubated, allowed to recover from anaesthesia in a 310 K incubator, and provided food and water *ad libitum*. Animal recovery, external signs of skin or tissue damage, and general behaviour were monitored.

At the appropriate time (~20 min before the 3, 9 or 25 h time elapsed, depending on the group) each mouse was re-anaesthetized, re-intubated, tethered in the imaging holder and re-mounted on the sample stage. After the imaging region was re-located (by matching as closely as possible to the corresponding baseline images, using a bony landmark for registration), one image was captured every ten breaths until a set of 110 images was collected (~10 min). After the repeat-imaging, the mice were humanely killed *via* Nembutal overdose without waking from anaesthesia, thus we did not attempt to limit the radiation dose at the second timepoint.

The tracheal tissue was excised and fixed in 10% neutral buffered formalin, and processed for wax histology and staining with haematoxylin and eosin. Tissue from the un-irradiated proximal trachea adjacent to the epiglottis was used as control tissue for the irradiated region.

2.3. Post-experimental analyses

All images were flat-field and dark-current corrected (Matlab R2012b; The Mathworks, Natick, MA, USA). Individual particle MCT rates were quantified using a Matlab program that presented an observer with 12 image frames (the first minute of either the baseline or repeat-imaging data, as appropriate) over which particle MCT was to be tracked. Images from the second baseline imaging period and the remaining 9 min of later repeat-imaging data were not used for this particular analysis. The observer was then prompted to manually track the location of a chosen particle *moving* through each of those 12 frames. The 12-frame sequence was then presented again, this time with the location of the previously tracked particle(s) shown, and the observer was prompted to track another particle. This process was repeated until a maximum of 50 particles were tracked, or until no additional moving particles could be identified in the sequence. This cycle was repeated for each animal (both baseline and repeat imaging), with the observer blinded to any information that would identify the group to which the animal belonged. The location of each of the selected points was stored in a spreadsheet. Separately, the location of every *stationary* particle (up to a maximum of 250 particles) in the first frame of each sequence was also recorded in a similar manner.

The pixel distance that each particle moved between each of the 12 frames was calculated and converted to millimetres based on the size of the field of view. The particle MCT rate was then calculated based on the time between analysis frames. A mean MCT rate and the total number of particles (either moving or stationary) were calculated for each time-point in every animal.

Statistical analyses were performed using *GraphPad Prism5*. Data were tested for normality, statistical significance was set at $p = 0.05$ and power = 0.80, and MCT rates were analysed by RM-ANOVA with Sidak's multiple comparisons or Kruskal-Wallis One-way ANOVA with Dunn's multiple comparisons, as appropriate. MCT rates are presented as mean and standard deviation [$\bar{X} \pm$ standard deviation (SD)].

3. Results

For the 24 animals studied here the mean time between dry particle insufflation and initiation of the imaging run was 5 min (SD 4 min), and involved setting up the mouse in the hutch and closing the hutch radiation door. The mean times between the baseline and repeat imaging were 3 h 4 min (SD 14 min), 9 h 36 min (SD 13 min) and 25 h 28 min (SD 11 min). The ion chamber output was used to estimate the photon flux and absorbed dose. For the baseline imaging a mean of 5.9 images (SD 4.5) was used to locate the imaging area. Combined with the 24 baseline image acquisitions this resulted in a mean dose of 1.35 Gy (SD 0.2). For the repeat imaging (after which the animals were humanely killed) a mean dose of 5.57 Gy (SD 0.74) was used. All mice survived the repeat-imaging protocol with no discernible adverse effects attributable to the baseline radiation exposure, regardless of the recovery period or dose delivered. Blinded histological analysis by an experienced research veterinarian also indicated that there was no difference in gross histomorphology to untreated animals.

Lead particles were immediately visible in the trachea of all animals when baseline imaging began, but the majority were stationary. An example of the identified particles is shown in Fig. 1; the top row shows the baseline and the bottom row shows the repeat-imaging. The number of particles delivered by the Dry Powder Insufflator™ was sufficient for distribution across the trachea, and for visualizing and quantifying MCT. For all rate analyses the limit of detection for MCT movement was ~0.02 mm min^{-1}. Fig. 2(*a*) shows the recorded MCT rate of every moving particle. A total of 48 moving particles were tracked at baseline, 25 at 3 h, 0 at 9 h and 2 at 25 h. The reduction in MCT rate at 3 and 25 h was statistically significant compared with baseline. Fig. 2(*b*) shows the same data but presented as an average MCT rate for each animal. This analysis did not show any statistically significant differences between the rates at each timepoint. As previously reported (Donnelley *et al.*, 2009, 2010, 2012), the *moving* particles followed unpredictable and non-linear paths along the airway. It was not possible to accurately identify the size, shape or surface properties of individual moving or stationary particles,

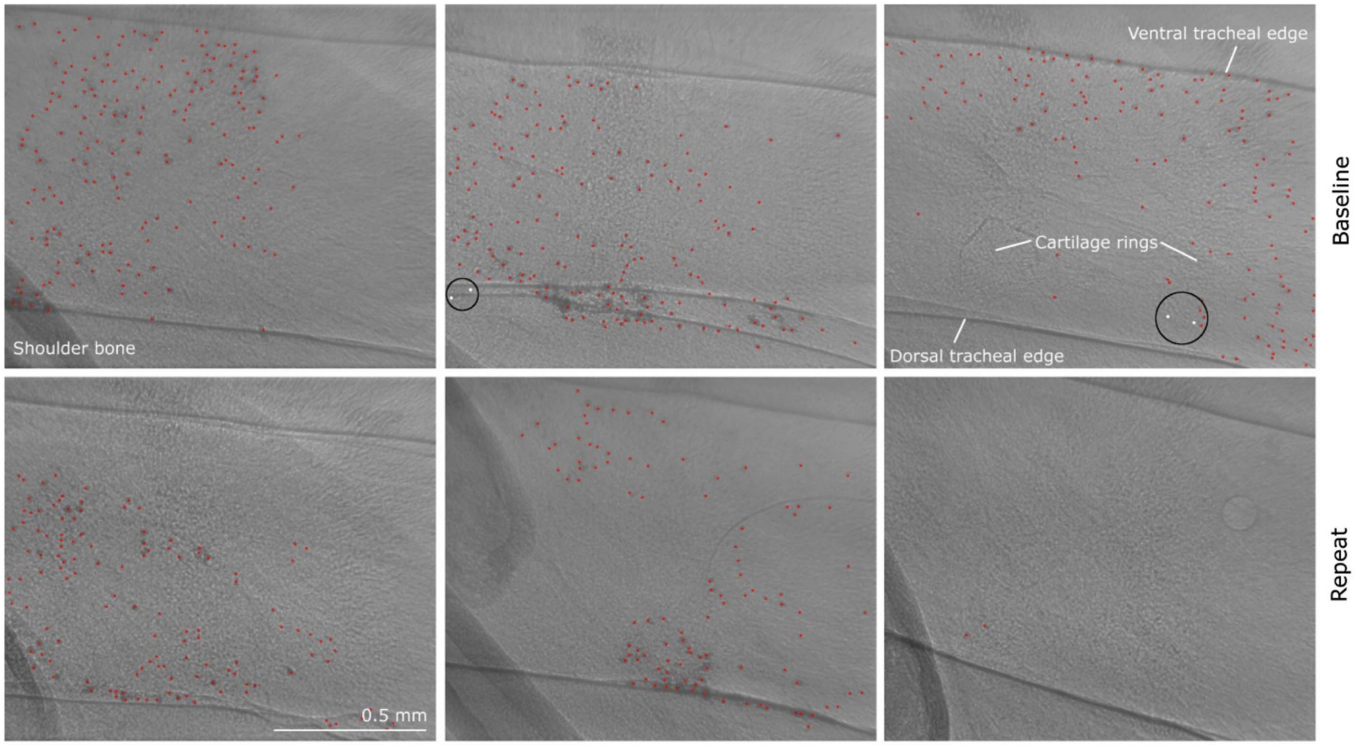

Figure 1
High-magnification images of lead dust in the trachea of three live mice (M1–M3) after particle insufflation, assessed using a repeat-imaging study design. The head is to the right and the spine is toward the bottom. The top row of images was taken at baseline, shortly after lead dust was delivered to the airway surface. The bottom row shows approximately the same locations (*a*) 3 h, (*b*) 9 h and (*c*) 25 h later. Imaging typically included the same bone edge (bottom left-hand corner) to help ensure that the same airway region was examined each time. Imaging location is just above the carina and the image dimensions are 1.45 mm × 1.2 mm. Stationary particles are marked in red and (the few) moving particles in white (black circles).

so we did not perform a quantitative analysis of these properties. However, subjectively it did not appear that particle size directly correlated with the rate at which the particles were cleared.

The total number of *moving* and *stationary* particles in every animal was also determined at each timepoint and is shown in Fig. 3. Although only a small number of *moving* particles were detected, many *stationary* particles were located in the first frame from each timepoint (these particles are marked red in Fig. 1). Notably, the number had halved after 3 h and were absent or very low at the later timepoints. Fig. 3 shows that while there was substantial variability in the number of particles detected at baseline, the mean number of particles in each group was similar. There were statistically significant reductions in the number of particles present at 9 and 25 h, but there was no difference at 3 h.

The ratio of the total particle count (*moving* and *stationary*) compared with baseline in each animal at each of the repeat-imaging timepoints is shown in Fig. 4. Each value was calculated by dividing the total number of particles in each animal at the repeat timepoint by the number present at baseline. Some mice contained more particles in the imaging region at the 3 h (n = 4 mice) and 9 h (n = 1 mouse) timepoints (*i.e.* proportion of baseline > 1). Significantly fewer particles remained at the 9 and 25 h timepoints compared with the 3 h timepoint.

4. Discussion

This study is the first report demonstrating the feasibility of repeat synchrotron X-ray imaging of MCT in live anaesthetized mice. Studies of this type will now allow changes in individual particle clearance to be visualized and quantified over extended periods of time after particle delivery. Minimizing the radiation dose delivered by reducing the number of exposures and the length of each exposure (while retaining a sufficient signal-to-noise ratio) is key to the success of repeat-imaging experiments of this type. Furthermore, the ability to reliably perform rapid and minimally invasive endotracheal intubations, a detailed knowledge of anatomical landmarks to facilitate rapid region of interest location, validation of appropriate marker particles, as well as stable and predictable anaesthesia within a remote delivery and physiological monitoring setting, are also essential.

High-resolution X-ray imaging requires large radiation doses to produce high-quality images. Although the radiation dose used in this study was high, it was localized to a very small area of the trachea ($\sim$1.7 mm^2), and did not pass through any other major anatomical structures or organs other than the skin and tissue surrounding the trachea. We did not observe any untoward physiological or histological effects in the mice over the study period, suggesting that this technique is appropriate for future studies of this type.

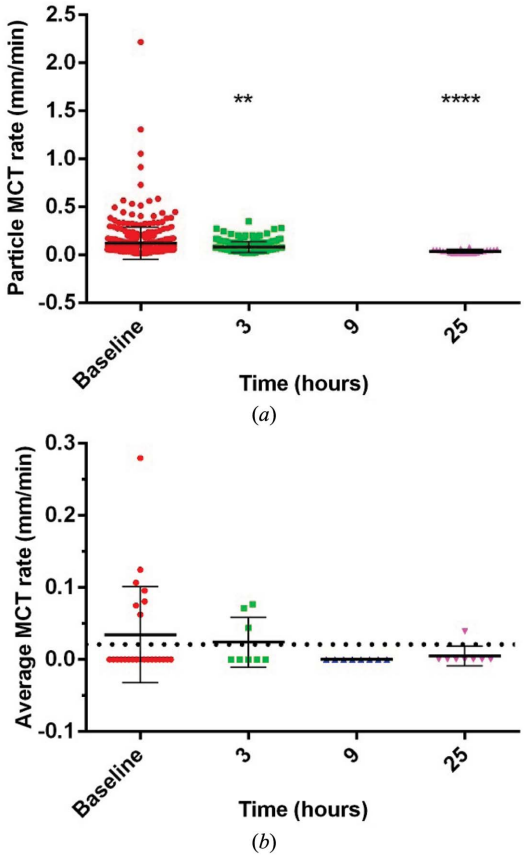

Figure 2
Characteristics of moving particles. (*a*) MCT rate of all detected moving particles at each timepoint. Note that no moving particles were detected at 9 h. The MCT rate at 3 and 25 h was significantly reduced compared with baseline. $^{**}p < 0.01$, $^{****}p < 0.0001$, Kruskal-Wallis One-way ANOVA with Dunn's multiple comparisons. (*b*) Average MCT rate for each animal across the study period. The limit of detection is marked with a dotted line.

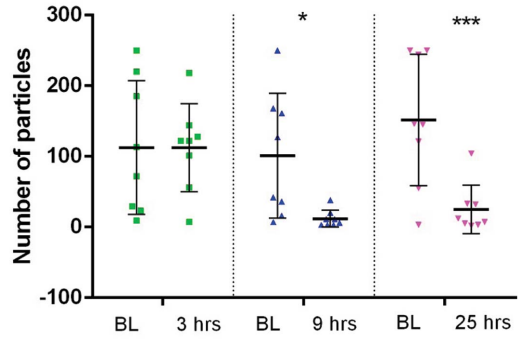

Figure 3
Total number of particles at each timepoint (moving and stationary). The total number of particles present at 9 and 25 h was significantly reduced compared with baseline (BL). There was no significant difference at 3 h. $^{*}p < 0.05$, $^{***}p < 0.001$ RM-ANOVA with Sidak's multiple comparisons.

Our results showed that the particle MCT rate decreases over time and that the number of particles present in the imaging region also decreases with time. Together this suggests that particle clearance continues to occur throughout the study period, but the particles remaining at the later timepoints take longer to clear because they are moving more slowly. This is consistent with the two-phase clearance process previously described (Falk *et al.*, 1999; Hofmann & Asgharian, 2003; Moller *et al.*, 2004). The lead dust used in this experiment had heterogeneous shape and surface characteristics, so it is possible that the particles that remained at the later timepoints may have been more tightly bound to surface mucus or trapped within the epithelial cell layer (Donnelley *et al.*, 2010).

The number of particles present at baseline also varied substantially between animals, suggesting that the Dry Powder Insufflator™ does not deliver a uniform quantity of dry particles despite being loaded in a similar manner prior to each actuation. The ability to accurately deliver small quantities of particles to the airways is desirable for this type of experiment; however, to account for this variability we calculated the proportion of particles present at the repeat timepoints compared with baseline (Fig. 4). This analysis showed that in some animals there were larger numbers of particles present in the trachea at the 3 and 9 h timepoints than at baseline, suggesting that clearance from the more distal conducting airways and alveoli was occurring. This was not the case at 25 h, and may suggest that the most mobile particles are all cleared within this time.

This study had a number of limitations. Firstly, although the radiation produced no detectable physiological effects, it may have been sufficient to produce transient radiation damage to the trachea and surrounding tissue, altering the MCT behaviour that we sought to measure. More complex studies should be performed in the future to elucidate this effect. Secondly, the number of particles delivered was both small and inconsistent, and the particles themselves varied in size, shape and surface properties. These factors would all influence the MCT rate of every recorded particle. We have already initiated studies using more uniformly sized and shaped particles to minimize this effect. Thirdly, during imaging the animals breathed dry imaging hutch air provided by the ventilator and this may have reduced the baseline MCT rate and subsequent clearance behaviour compared with air that is normally humidified by transit through the mouse nasal airways.

The timepoints chosen were limited by the two days of available beam time at the SPring-8 synchrotron. In future

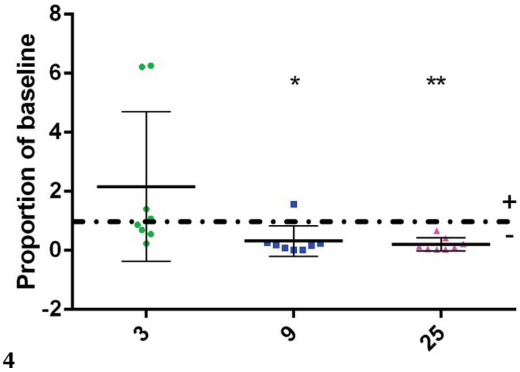

Figure 4
Proportion of particles (moving and stationary) at each repeat imaging point, compared with baseline. Significantly less particles remained at 9 ($^{*}p < 0.05$) and 25 h ($^{**}p < 0.01$) compared with at 3 h. Kruskal-Wallis One-way ANOVA with Dunn's multiple comparisons.

studies we plan to use larger groups of mice with more time-points extending for longer periods to more thoroughly examine how MCT occurs over time. Furthermore, we plan to also test common clinical rehydrating treatments for CF, such as hypertonic saline and mannitol, to determine how they affect the long-term clearance of particulates.

In summary, these studies have shown that it is now possible to perform repeat synchrotron X-ray imaging studies. The ability to perform repeat-imaging experiments may have applications in further understanding the physiological and physical basis of inhaled particle clearance and testing the efficacy of pharmaceuticals designed to improve MCT.

These studies are supported by the Women's and Children's Hospital Foundation, NHMRC Australia (project 626863) and philanthropic donors *via* the Cure4CF Foundation (http://www.cure4cf.org). The synchrotron radiation experiments were performed on the BL20XU beamline at SPring-8, with the approval of the Japan Synchrotron Radiation Institute (JASRI) under proposal number 2012A1661. We thank Professor Naoto Yagi, Dr Kentaro Uesugi, Dr Yoshio Suzuki and Dr Akihisa Takeuchi (SPring-8) for their assistance with the experimental set-up, Ms Chantelle McIntyre and Dr John Finnie for histological analysis, and Dr Stuart Howell (University of Adelaide) for his assistance with the statistical analyses. MD is supported by a MS McLeod Fellowship, KM by an ARC DECRA, AF by a NHMRC CDF, and NF by a MS McLeod PhD Scholarship. All authors were supported by the Australian Synchrotron International Synchrotron Access Program (ISAP). The ISAP is an initiative of the Australian Government being conducted as part of the National Collaborative Research Infrastructure Strategy.

References

Boucher, R. C. (2004). *Eur. Respir. J.* **23**, 146–158.
Chodhari, R., Mitchison, H. M. & Meeks, M. (2004). *Paediatr. Respir. Rev.* **5**, 69–76.
Cloetens, P., Barrett, R., Baruchel, J., Guigay, J. P. & Schlenker, M. (1996). *J. Phys. D*, **29**, 133–146.
Coan, P., Wagner, A., Bravin, A., Diemoz, P. C., Keyriläinen, J. & Mollenhauer, J. (2010). *Phys. Med. Biol.* **55**, 7649–7662.
Donaldson, S. H., Corcoran, T. E., Laube, B. L. & Bennett, W. D. (2007). *Proc. Am. Thorac. Soc.* **4**, 399–405.
Donnelley, M., Morgan, K. S., Fouras, A., Skinner, W., Uesugi, K., Yagi, N., Siu, K. K. W. & Parsons, D. W. (2009). *J. Synchrotron Rad.* **16**, 553–561.
Donnelley, M., Morgan, K. S., Siu, K. K., Farrow, N. R., Stahr, C. S., Boucher, R. C., Fouras, A. & Parsons, D. W. (2014). *Sci. Rep.* **4**, 3689.
Donnelley, M., Morgan, K. S., Siu, K. K. W. & Parsons, D. W. (2012). *J. Synchrotron Rad.* **19**, 551–558.
Donnelley, M., Siu, K. K. W., Morgan, K. S., Skinner, W., Suzuki, Y., Takeuchi, A., Uesugi, K., Yagi, N. & Parsons, D. W. (2010). *J. Synchrotron Rad.* **17**, 719–729.
Falk, R., Philipson, K., Svartengren, M., Bergmann, R., Hofmann, W., Jarvis, N., Bailey, M. & Camner, P. (1999). *Exp. Lung Res.* **25**, 495–516.
Grubb, B. R., Jones, J. H. & Boucher, R. C. (2004). *Am. J. Physiol. Lung Cell. Mol. Physiol.* **286**, L588–L595.
Hofmann, W. & Asgharian, B. (2003). *Toxicol. Sci.* **73**, 448–456.
Hua, X. Y., Zeman, K. L., Zhou, B. Q., Hua, Q. Q., Senior, B. A., Tilley, S. L. & Bennett, W. D. (2010). *J. Appl. Physiol.* **108**, 189–196.
Livraghi, A. & Randell, S. H. (2007). *Toxicol. Pathol.* **35**, 116–129.
Moller, W., Haussinger, K., Winkler-Heil, R., Stahlhofen, W., Meyer, T., Hofmann, W. & Heyder, J. (2004). *J. Appl. Physiol.* **97**, 2200–2206.
Snigirev, A., Snigireva, I., Kohn, V., Kuznetsov, S. & Schelokov, I. (1995). *Rev. Sci. Instrum.* **66**, 5486.
Wilkins, S. W., Gureyev, T. E., Gao, D., Pogany, A. & Stevenson, A. W. (1996). *Nature (London)*, **384**, 335–338.